RESEARCH PAPER

Chemical Vapor Deposition Synthesis of Novel Indium Oxide Nanostructures in Strongly Reducing Growth Ambient

Ashish Karn [1], Nitesh Kumar [2] and Sivanandam Aravindan[3]*

[1] *St. Anthony Falls Laboratory, University of Minnesota Twin Cities, Minneapolis, MN, USA*

[2] *Yale University, Whitney Avenue, New Haven, CT, USA*

[3] *Indian Institute of Technology Delhi, Hauz Khas, New Delhi, India*

ARTICLE INFO

Article History:
Received 28 November 2016
Accepted 21 September 2016
Published 01 January 2017

Keywords:
Chemical Vapor Deposition
Growth ambient
Hydrazine
Indium Oxide

ABSTRACT

The current study reports some interesting growth of novel In_2O_3 nanostructures using ambient-controlled chemical vapor deposition technique in the presence of a strongly reducing hydrazine ambient. The experiments are systematically carried out by keeping either of the carrier gas flow rate or the source temperature constant, and varying the other. For each of the depositions, the growth is studied at three different locations downstream. In this paper, we report the growth of some novel nanostructures including nanodonuts, nanomushrooms, standing nanorods and long nanowires using ambient controlled chemical vapor deposition technique. Further, the nanostructures are characterized through scanning electron microscopy, transmission electron microscopy and x-ray diffraction. First, the growth of nanowires, octahedral and nanorods were verified to occur in oxidizing, inert and reducing ambient, respectively. However, a systematic variation of experimental parameters shows that different kinds of nanostructures can be obtained using highly reducing hydrazine ambient. Further, simultaneous growth of octahedral along with nanomushrooms and the hexagonal tip of the standing nanorods provides some insight into the growth mechanisms of these novel nanostructures. Possible growth mechanisms of the nanostructures are also discussed in detail.

How to cite this article
Karn A, Kumar N, Aravindan S. Chemical Vapor Deposition Synthesis of Novel Indium Oxide Nanostructures in Strongly Reducing Growth Ambient. J Nanostruct, 2017; 7(1): 64-76. DOI: 10.22052/jns.2017.01.008

INTRODUCTION

Low dimensional oxide nanostructures have densely packed oxygen vacancies on the surface, large surface-area-to-volume ratios, and lateral dimensions which are about the order of the thickness of gating charge layer in field effect transistors [1]. These nanostructures have shown great promise in chemical and biological sensors [2-6], viz. Indium oxide nanowires have shown greater room temperature sensitivity than their commercial tin-oxide thin film sensors. Indium oxide (IO) has been suggested as a highly sensitive gas sensor toward target gases such as CO [7], NH_3 [8], NO_2 [9], H_2 [10] and H_2S [11,12]. IO is a semiconductor with a wide band gap (direct band gap of 3.75 eV) which becomes highly conductive upon doping with valence cations [13]. Oxygen vacancies are another source of conducting electrons, accounting for the low resistivities of undoped, oxygen deficient materials. Owing to their wide band gap and high transparency in the visible region, Indium Oxide nanostructures are attractive for several applications in nanoelectronics and optoelectronic devices [14].

* *Corresponding Author Email: karn@umn.edu*

IO nanostructures have been investigated for a multifarious range of applications viz. Sensors [2-6], transparent thin film transistors [15], dye-sensitized solar cells [16] field-effect transistors [17], and waveguides [18]. Different morphologies of IO nanostructures have different applications, such as nanowires for optoelectronics, efficient field emission, biosensors, nanoparticles for toxic gas sensing, single-crystalline IO pyramids for efficient field emission etc. So it is important to explore a rational experimental route to synthesize various nanostructures for meeting different requirements in future nanodevices.

It is well known that the structure and morphology of materials plays an important role in its physical properties. The size and morphology dependencies of optical, catalytic, magnetic and transport behavior has been extensively studied. As size reduction of materials at the nanoscale has inevitably led to the discovery of novel properties and thus opened up new opportunities for different applications of the materials, various low-dimensional nanostructures of IO have been investigated. Thus, there is increasing interest in the synthesis and property investigation and study of growth mechanism of low-dimensional IO structures.

IO nanostructures have generally been synthesized by well-known thermal evaporation methods, including carbothermal reduction [19], vapor transport and condensation [14], metalorganic chemical vapor deposition [20] etc. These have also been synthesized by other methods such as laser ablation, electrodeposition [21] hydrothermal synthesis [22] and solvothermal followed by annealing [23]. Various IO nanostructures have been fabricated by vapor and solution routes, such as nanobelts, nanowires, bamboo-like wires, multi-kinked wires, nanospirals, nanocontainers and mesocontainers [14], nanoparticles (octahedron, pyramids and cubes), nanobouquets and nanotrees, nanotubes and nanotubes filled with indium, hollow spheres, nanotowers, nanochains etc. However, investigating novel nanostructures is still an important task, because they provide not only a deeper understanding of material growth but also functional materials for advanced technological applications.

Among the synthesis methods, vapor transport is a powerful method and the obtained product often shows good crystallization. In the vapor route, the morphologies of products can be modulated through changing the experimental conditions, such as source materials, temperatures, carrying gas etc. It is important to study the relation between the experimental conditions and the morphologies. CVD is a facile and very convenient process and it would be immensely useful if experimental modulation in such a simplistic process can yield a diverse array of morphologies that may be useful in future nanodevices. Towards this end, understanding of the growth mechanism and its dependence on deposition parameters, essential for tunable morphological synthesis of IO nanostructures will be quite useful. However, there are only a few reports on novel morphologies like standing rods, kinked wires etc. using CVD growth. Although the prior studies have focused on the variation in growth morphologies for inert, mildly oxidizing and reducing ambient, systematic studies upon the effect of a strongly reducing ambient like hydrazine has not been conducted. Moreover, the growth of novel Indium oxide morphologies like nanodonuts, nanomushrooms etc. have not been reported yet and the growth mechanism of these structures have received very little attention, if at all.

Here, we report a holistic approach using CVD technique on a gold deposited (100) Silicon substrate by introduction of Hydrazine ambient to achieve the controlled synthesis of a wide variety of IO nanostructures, which include nanodonut web, nanomushrooms, Standing rods, Multi-kinked wires, Ultra long nanowires, Inter-penetrating rods and multipods, Nanowhiskers, High aspect ratio rods etc. The characterization of these nanostructures is done and a possible growth mechanism is discussed.

MATERIALS AND METHODS

The schematic of the thermal vapor transport technique employed to grow the IO nanostructures is shown in Fig. 1. The system consists of microprocessor controlled single zone high temperature furnace with maximum attainable temperature of 1473K and temperature accuracy of 1K, quartz tube with outer diameter 55mm, inner diameter of 50 mm and length of 1000mm, rotary pump and mass flow controller. There is a central heating zone and temperature on both sides of the tube decreases. The aluminium coupler was connected at both the ends of the tube with cooling arrangement; it was connected to the inlet

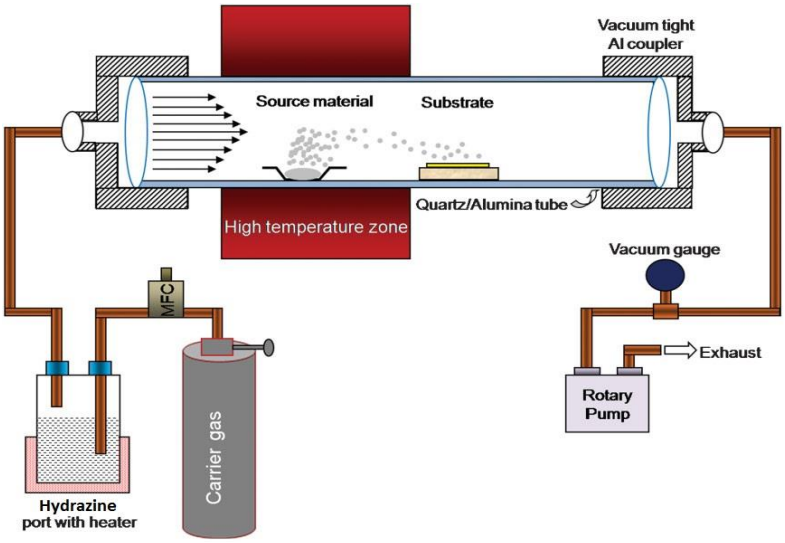

Fig. 1. Schematic of thermal CVD set-up used for the growth of IO nanostructures (Adapted from [3])

of carrier gas. The carrier gas flow was controlled by mass flow controller and the desired amount of gas was supplied directly in the reaction tube or passed through ambient vapor. A small reservoir for creating the desired ambient was kept in the upstream direction of the tube and contained water/ethanol etc. The other end of the tube was connected to the rotary pump through Al coupler for creating the vacuum. The vacuum gauge was connected at the rotary end to measure the pressure in the tube during growth.

Single crystal (1 0 0) silicon wafers were used as substrates. 5 nm Au thin film was deposited on the Si substrates using thermal evaporation under high vacuum conditions. The wafers were cleaned by dipping in dilute HF solution (HF/H_2O= 1:10) and sonicating for 2 min to remove the top layer of silicon dioxide that gets formed on the exposure of silicon to atmosphere. They were then washed with distilled water and propanol and finally dried under a hot jet.

Growth was carried out in a single zone horizontal quartz tube furnace at atmospheric pressure. A ceramic boat containing IO powders and graphite (1:1 weight ratio) were introduced into the central heating zone of the furnace, which was maintained at a source temperatures of 900-1200 ^{0}C. The Silicon substrates were placed downstream on boat and at a distance of one and two inches from the boat. The range of substrate temperatures for three different source temperatures are shown in the Fig. 2. The powders were held at a particular temperature for 1 hour. After the experiment, the gas flow was continued for 20 minutes and the furnace was cooled to room temperature. During the experiment, the argon gas was passed through the furnace at different flow rates in the range of 50-200 Sccm along with hydrazine hydrate vapors.

Total three sets of experiments consisting of six depositions were carried out, as enlisted in Table 1. In first experiment (deposition I and II), the argon flow rate was kept constant and the depositions were done for two temperature values of 900 and 1000°C. Next, the temperature was kept fixed at 1000°C and the carrier gas flow rate was varied from 50 Sccm to 200 Sccm. Finally, the effect of temperature variation was explored again at a larger Argon gas mass flow rate of 200 Sccm. A white product was found to deposit on the surface of the plate and the inner wall of the boat. The morphological, structural and compositional characterization was carried out by scanning electron microscopy (SEM; Ziess EVO 50), field emission scanning electron microscopy (FESEM) (Quanta 200F), X-ray diffraction (XRD) (Phillips X'Pert, PRO-PW 3040) with Cu Kα radiation at a scanning rate of 0.02° s-1 in a 2θ range of 20-80° and high resolution transmission electron microscopy (HRTEM; Tecnai G20-Stwin at 200kV) at 200 kV. The elemental analysis was carried out using energy dispersive X-ray (EDX) spectroscopy attached with the TEM and FESEM.

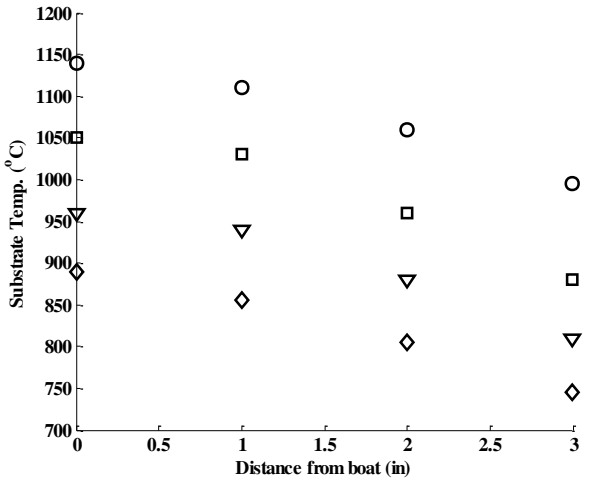

Fig. 2. Temperature Variation with respect to distance from the boat for three different source temperatures. Circles, squares, triangles and diamonds correspond to a source temperature of 1200, 1100, 1000 and 900, respectively.

RESULTS AND DISCUSSION

For all the cases mentioned above, the depositions were carried out at three different locations: on the boat, and at a distance of one and two inches away from the boat. After the deposition, each substrate was characterized through X-ray diffraction technique (XRD), scanning electron microscopy and transmission electron microscopy.

XRD Characterization

The phase and purity of the sample were confirmed by XRD pattern. Fig. 3 shows the X-ray diffraction spectra of the obtained products. The diffraction peaks in the Fig. 3 correspond to (222), (400), (411), (422), (444) and (820) planes, which can be indexed to body-centred cubic (bcc) IO single crystal with a lattice constant of a= 1.011 nm (JCPDS card No. 06-0416). No other impurity phases such as Indium were detected. The unidentified peak at 53.5° corresponds to silicon substrate. The strong and sharp diffraction peaks indicate that the as-obtained product is well-crystalline.

Structural characterization

The first step in the growth of nanostructures was the optimization of the experimental parameters which led to growth of nanostructures. Our experiments revealed that generally the growth of nanowires and other morphologies is significant for source temperatures higher than 1000^0 C. Prior studies have revealed the dependence of the nanostructure morphology on the growth ambient in the vapor phase transport technique [24]. Thus, similar ambient conditions were employed in our experiments to determine the optimal location of the substrate with respect to boat and obtained nanostructure morphologies were observed using SEM. Fig. 4 below presents the SEM images of the obtained nanostructures under different ambient.

In all the three cases, nanostructure growth was found to occur on the boat and at a distance of one and two inches, however no substantial growth was observed further downstream. Thus, these three locations were chosen for deposition of IO nanostructures under hydrazine ambient.

Table 1. Details of all the experiments performed

Deposition No.	Carrier gas flow rate (Sccm)	Source Temperature (^{o}C)
I	50	900
II	50	1000
III	125	1000
IV	200	1000
V	200	1100
VI	200	1200

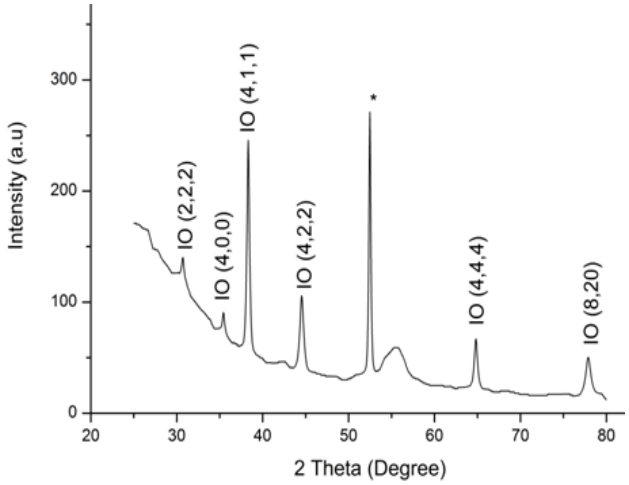

Fig. 3. A typical XRD spectra of IO nanostructures deposited under depositions I-VI by the vapor phase transport technique. The XRD spectra have contributions from IO nanostructures and material underlying IO on the silicon substrate. The arrows indicate respective peaks. The unmarked peaks are of Silicon.

Two different categories of experiments were performed. In one of the categories, substrate temperature was held constant at 1000°C and the carrier gas mass flow rates were varied from 50 to 200 Sccm (deposition # II, III and IV). In the second category, the carrier gas mass flow rates were fixed and the effect of variation in source temperature was explored. The experiment in second category was repeated both at low values of carrier gas flow rate (deposition # I and II at 50 Sccm) and high carrier gas flow rate (deposition # IV, V and VI at 200 Sccm).

Exploring the effect of Carrier gas mass flow rate

The variation in carrier gas flow rate was studied at a fixed source temperature of 1000 °C for three different values of argon mass flow rate. Fig. 5 presents an array of SEM micrographs of nanostructures grown using the same pressure, substrate, and deposition temperature but at

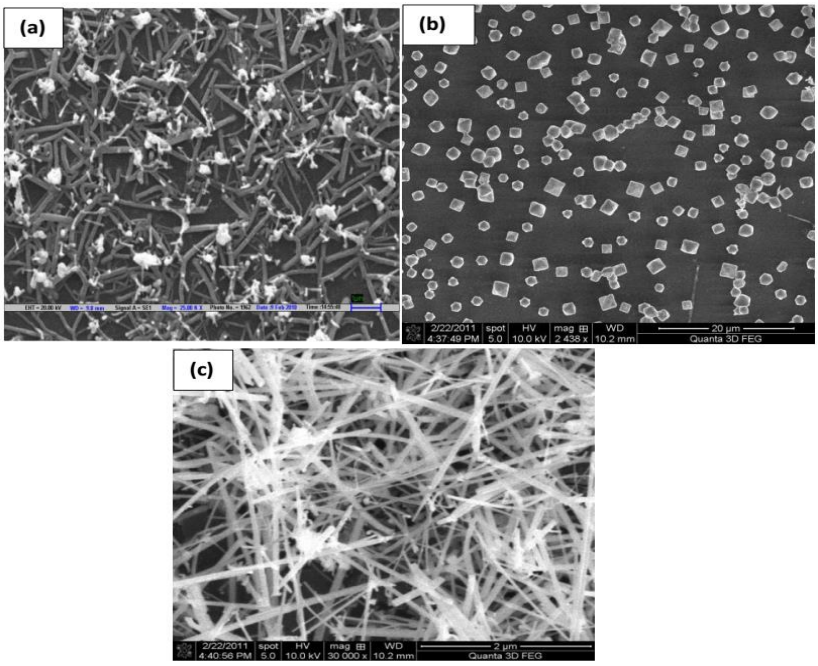

Fig. 4. FESEM micrographs of (a) Nanorods grown under ethanol ambient, (b) Octahedra grown under inert ambient, and (c) Nanowires grown under the ambient of water vapor. Scales shown on the Fig. correspond to 1μm, 20 μm and 2 μm, respectively.

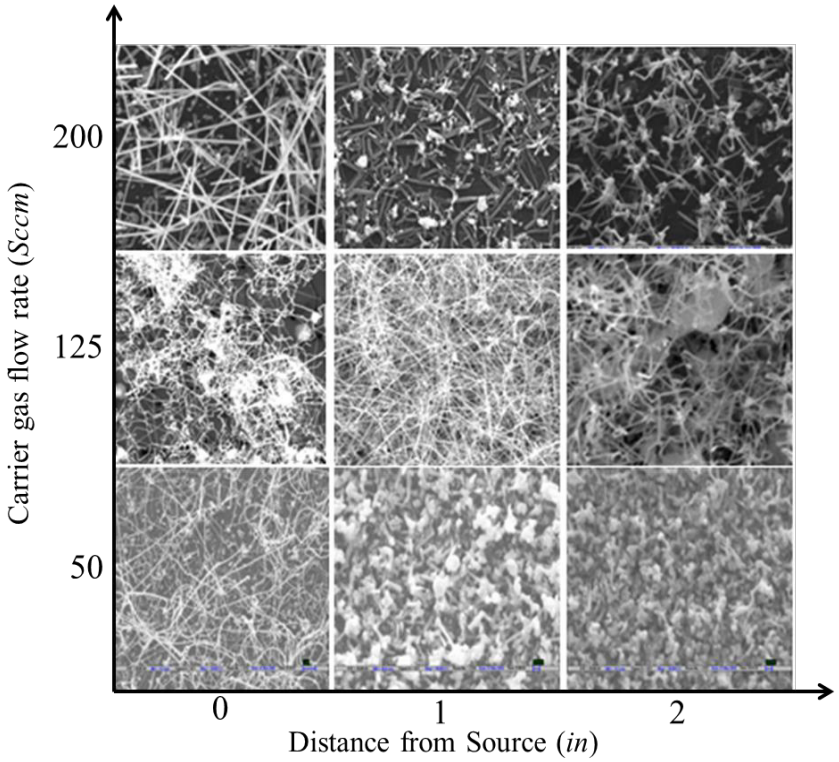

Fig. 5. SEM micrographs of the nanostructures grown at 1000 °C for various Sccm values at different distances from the boat.

different values of Argon gas flow rates. In general, it is observed that the morphology of the IO nanostructures is mainly affected by the carrier gas flow rate, whereas the reaction temperature changes only the diameter of the IO nanowires. The change in the carrier gas flow rate had a negligible effect on the cross-sectional area of the nanowires.

At a lower flow rate of 50 Sccm, high aspect ratio nanowires with aspect ratios greater than 1000 are obtained on the boat. These wires have diameters in the range of 50±10 nm and their lengths fall in the range 60±20 µm. At a distance of 1 inch from the boat, the morphology changes to Nanorods and multi-pods, with each arm having length in the range of 5±2 µm and their average diameters in the range of 50±5 nm. These nanorods further penetrate into each other and give inter-penetrating rods at a lesser substrate temperature of 880°C. When the Argon gas flow is increased by 75 Sccm, the nanowires get "kinked" resulting in the formation of multi-kinked nanowires and other kinked structures. The growth on boat is a web of multi-kinked wires and at the distance of one inch, kinked wire-decorated nanowires are observed. Although straight, these nanowires are intermittently decorated with a web of kinked wires. Agglomeration of kinked wires is observed at a further distance from the boat. When the Argon flow rate increases to 125 Sccm, the precipitation and oxidation processes become so much faster that constituent atoms have not enough time to diffuse and form clearly faceted nanowires, and hence the produced nanowires have a bent morphology, as shown in Fig. 6. The TEM and HRTEM images of bent IO nanowires show that they have a rough surface and no unique growth direction. These results also indicate that more defects can be introduced in the surface of the bent nanowires. It is generally accepted that the bent and curved nanowires contain localized defects at the bending regions and surface.

At very high values of flow rates (200 Sccm), nanowires with aspect ratios around 100 are obtained, their diameters in the range of 60±20 µm and lengths in the range of 5±1 µm. At a lower substrate temperature, short and thick nanorods with their diameters in the range of 250±50 nm and their lengths in the range of 2-4 µm are obtained. At a further lower substrate temperature, multi-

pods like structures interwoven with nanowire web is obtained. The nanorods which have diameters in the range of 160 ± 10 nm and lengths of about 3-4 µm are found to have their one end joined and the nanowires have high aspect ratios. It is interesting to note that in all the three cases, there is a location where high aspect ratio nanowires web are obtained and this optimum distance gets pushed downstream with increase in carrier gas mass flow rate. From Fig. 5 it can also be noticed that on moving downstream, there is a tendency of agglomeration and inter-penetration. It can be very easily observed that as the mass flow rate of the carrier gas increases, the growth density reduces because the concentration of growth species is reduced. Similarly, it can also be observed that at higher gas flow rates, the thickness of nanostructures increases. This may be due to stacking of the rods or wires at higher flow rates. Carrier gases can change the structures of nanostructures. The reason for the formation of different structures is related to the growth rate induced by the different carrier gases at different flow rates. It is possible that this is due to the combined influence of the growth rate, super saturation and the structural properties of the catalytic nanoparticles. It is also possible that gases like N_2 could induce additional chemistry that changed the nanostructures. For instance, AuN thin films may form leading to less growth density or, there could be a possibility of formation of InN nanostructures. However, the mechanisms involved have still not been clearly ascertained and require further investigations.

Exploring the effect of Substrate Temperature

The growth at constant carrier gas flow rate was carried out in two separate regimes: high temperature and low temperature. Low temperature regime had a temperature of 900 and 1000 °C whereas high temperature regime consisted of temperature of 1100 and 1200 °C. It was observed that the growth in the high temperature regime (at 1200 °C) was drastic and probably involves some self-assembly mechanism. However, growth till a temperature of 900-1100°C can be controllably carried out.

As Fig. 7 shows, at a lower temperature of 900 °C, growth is relatively sparse because at a low temperature probability of nucleation is less. So, lesser number of nuclei is formed leading to less density. Even then, all the nuclei that are formed may not result into nanostructure growth probably because the low source temperature doesn't lead to the formation of enough source vapor formation (large number of nucleation sites can be seen) and the surface migration is also low. As the lateral diffusion is suppressed at low temperatures, the axial growth is faster and hence the nanowire growth is faster, compared to nanorods. The Fig. 7 shows the nanorods of length 1.5±0.5 µm and diameter of around 125 nm. The nanowire whose density is more is longer (<7 µm) and thinner (D < 35 nm).

At a distance of one inch from the boat, i.e. at a slightly lower temperature, we can observe the formation of standing nanorods. It is notable that the standing nanorods of Indium Oxide have not yet been reported in the literature through CVD technique. Interestingly, as shown in the Fig. 8, these rods although cylindrical have a hexagonal faceted tip, which has not been reported. Generally, the presence of the gold at the tip indicates the VLS growth mechanism, but this kind

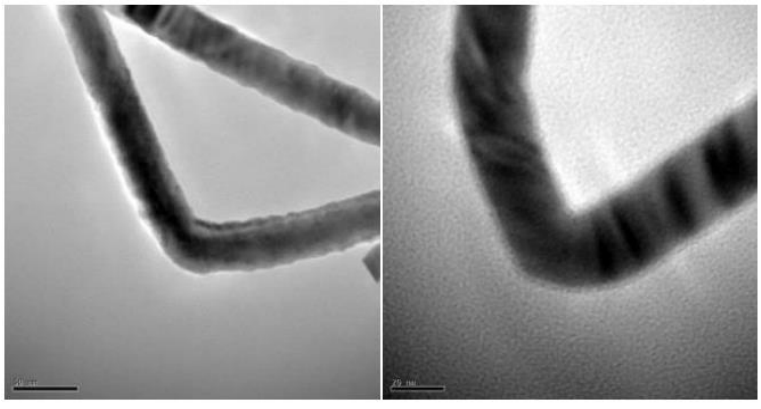

Fig. 6. TEM image of the bent and kinked nanowires obtained at 125 Sccm.

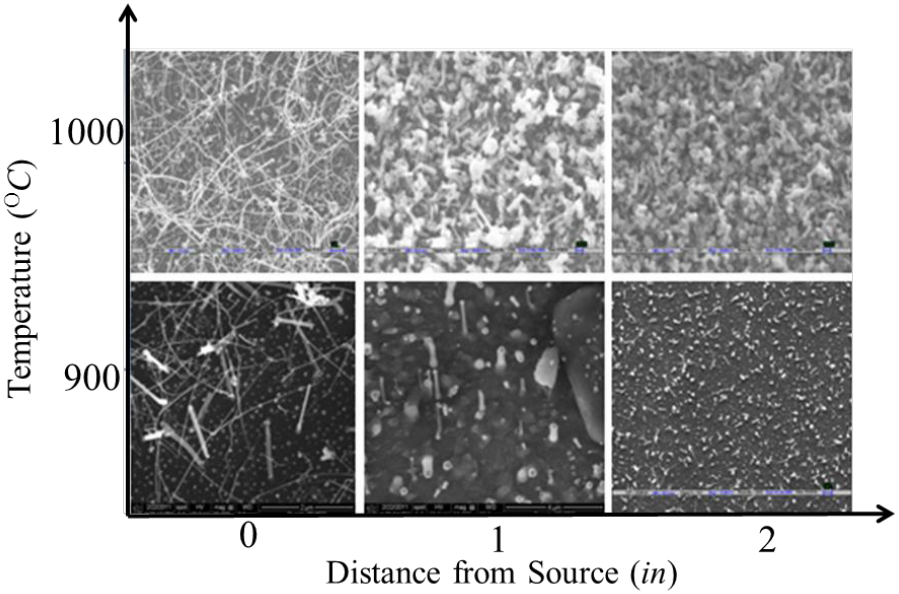

Fig. 7. SEM micrographs of the nanostructures obtained at a lower Sccm value of 50 Sccm and at lower temperature ranges of 900 and 1000 °C at different distances from the boat

of tip bears an indication to the VS or some other mechanism. It can be argued that the standing rod formation takes place due to two primary reasons: First, the slow growth rate at these temperatures gives sufficient time for lateral diffusion to take place and thus form a thicker base. Also, the lower value of gas flow rate ensures that there is enough time for deposition and the growing rod can stand rather than getting bent. The formation of the hexagonal top and the exact growth mechanism is yet unknown. The growth at two inches is sparse of course, due to the depletion of the reactant species.

This is especially important since the orderliness of size depending on the growth temperature may have an important reference in the controlled growth of functional nanodevices with special size demands. Surface diffusion of adsorbed species on the substrate surface and on the surface of the grown surface is also temperature dependent. The partial pressure of the reagent species affects super saturation during the growth of nanostructures. At higher reaction temperature, the Au layer on the Si substrate tends to agglomerate and form larger catalyst particles at the tip of the nanowires. Thus, the diameter of the IO nanowires increases with the reaction temperature.

The success of our experiments is guided by the Nucleation theory. The probability of nucleation is given by:

$$P_n = A \exp(\frac{-\pi\sigma^2}{T^2 k^2 \ln \alpha})$$

Where A is a constant, σ is the surface energy, α − 1 is the supersaturation, where α = p/po. In this case p is the vapor pressure of the growth species, po is the equilibrium vapor pressure of the condensed phase, k is the Boltzmann constant, and T is the temperature in Kelvin. In other words, at constant growth conditions, T and assuming a constant surface energy (σ) throughout the experiment, it is possible to enhance α and the nucleation probability (P_n). At decreased growth temperatures, the nucleation probability P_n, and the surface migration will be suppressed. Thus if the growth temperatures are low enough to to suppress migration along the 2D surface of the c-plane but high enough to sustain the growth along the c-axis, the condensation and growth will be limited.

The growth in the higher temperature regime at a higher carrier gas flow rate is more interesting, as it involves several factors. In this process, there are two crucial factors determining the growth behaviour of crystals: mobility and mean free path of absorbed reagent species. The mobility depended on the growth temperature, and under high temperature, the molecular kinetic energy

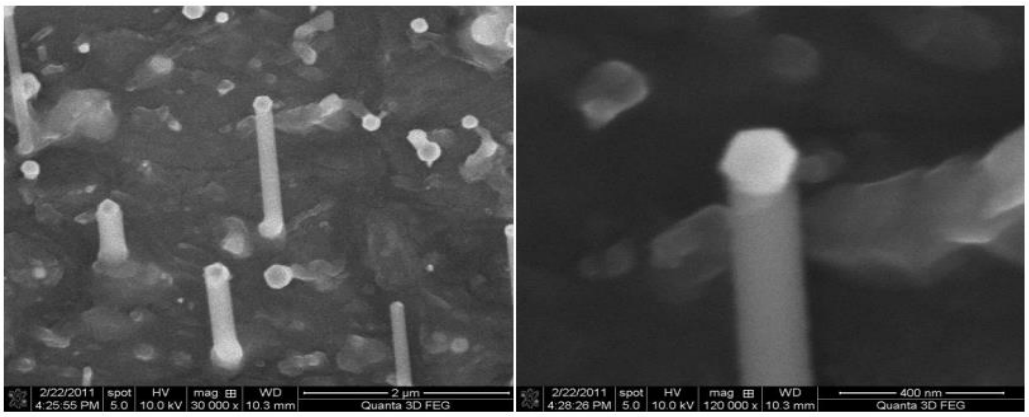

Fig. 8. FESEM micrograph of standing nanorods grown under Hydrazine Anbient

was high and these absorbed species would have high mobility. As for the mean free path, which was determined by the super saturation ratio, under a high super saturation ratio, the opportunities of the absorbed species impinging on each other would increase and the mean free path would decrease. In this experiment, the distinction of reagent super saturation ratio along the flow direction was small because of the large flow rate (200 Sccm). It indicated that the mean free path of reagent species upon four Si substrates was approximately the same. So the influence of super saturation on the growth behaviour was a secondary factor. Thus, the growth temperature resulted in the evolution of configuration. From Fig. 9, it may be argued as to why the long nanowires are produced at two inches from the boat for the temperature of 1100 and 1200 °C whereas for the case of 1000 °C, the long nanowire growth is on boat. This can be explained on the basis of optimum availability of Au and IO vapor.

The Au film on substrate at one inch will start to evaporate because of the volatile near-surface atoms of the Au nanoparticles at high temperatures (melting point of bulk Au is 1064.43 °C but is lower for thin films and nanoparticles). According to Fick's law, the diffusion flux J = -D(dN/dx), where J is the net flux of vapors (per unit area in unit time), D is the diffusion constant, and (dN/dx) is the concentration gradients of the vapors along the propagation direction x. This means that the diffusion will always propagate to a region with lower Au and IO vapor concentration. Nanowires have the longest lengths and more uniform diameters probably because of the optimum Au and IO vapor concentrations. Apparently, due to the Au vapor mediated growth, the nanowires are so longer, without which the IO will condense as short nanorods. The mechanism of this success is the introduction of controlled concentration gradients of InO and Au vapors. It can be conjectured that a similar mechanism could be applicable to control Au and InO vapors for selective growth of other InO nanostructures.

Growth Mechanism

Four sequential steps can be identified in the growth of a crystal: (1) transport of the reagent species in the vapor phase; (2) absorption of reagent species onto the surface of the nucleus; (3) transfer of absorbed species along the surface of nucleation; (4) precipitation, incorporation, and crystal growth.

The first step is carbothermal reduction of Indium oxide:

$$IO\ (s) + C\ (s) \rightarrow In_2O\ (v) + CO_2\ (v)$$

Further reduction of reaction species into indium rich ambient takes place

$$2\ In_2O\ (v) + N_2H_4\ (v) \rightarrow 4\ In\ (v) + N_2\ (g) + 2\ H_2O\ (v)$$

Also, Indium oxide may directly be reduced to Indium vapor by the strongly reducing hydrazine:

$$2\ IO\ (s) + 3\ N_2H_4\ (v) \rightarrow 4\ In\ (v) + 3\ N_2\ (g) + 6\ H_2O\ (v)$$

Indium vapor or In_2O vapor may be trapped by the liquid alloy and thus converts into liquid:

$$In\ (v) / In_2O\ (v) \rightarrow In\ (l) / In_2O\ (l)$$

Subsequently, In (l) or In_2O (l) absorbs oxygen to get converted to In_2O_3 (s) before getting deposited:

$$In\ (l) / In_2O\ (l) + O_2\ (g) \rightarrow In_2O_3\ (s)$$

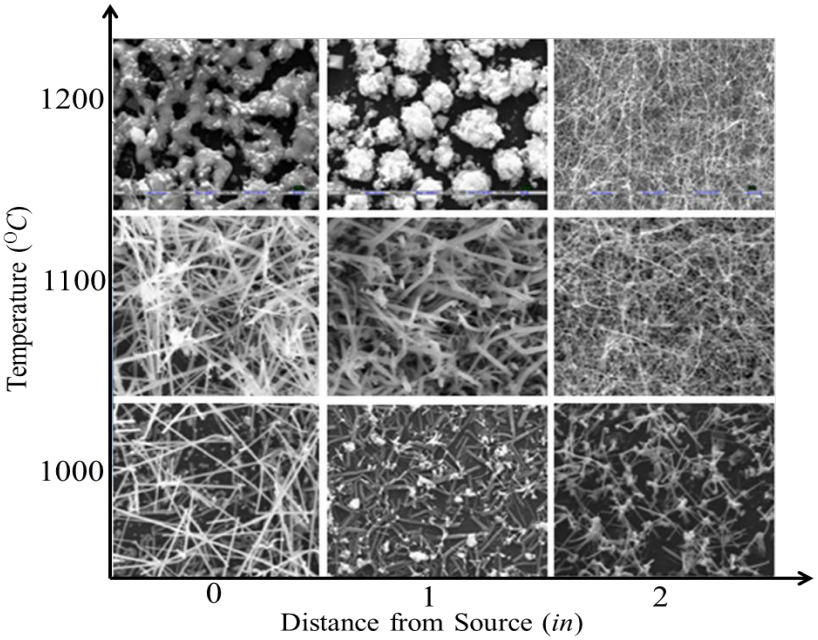

Fig. 9. SEM micrographs of the nanostructures obtained at a higher carrier gas mass flow rate (200 Sccm) and in higher temperature range at different distances from the boat

Nanodonut formation

Nanodonuts have not very frequently been reported in the literature though novel ZnSe Nanodonuts have been prepared by surfactant assisted methods. However, there have been no reports on the growth of either IO Nanodonuts or nanodonut growth through CVD technique. At high temperature the growth is very drastic and unpredictable because the possibility of self-assembly mediated growth. There have been several reports on the self-assembly growth in the literature. One such growth of IO tubular structures was reported by Zhong et al [25]. Fig. 10 shows the growth of nanodonut like morphology at different magnification (the red circles are to facilitate the identification of coalescence sites). It can be very clearly seen that the growth of Nanodonut is a very uniform and isotropic one covering the entire substrate (see Fig 10 (a)). It is observed that the inner diameter of these nanodonut web structures varies from 100-400 nm and the thickness of the donut is 100 nm. Since Surface diffusion of adsorbed species on the substrate surface and on the surface of the grown surface is also temperature dependent. It can be speculated that at higher temperatures the self-assembly of nanorods favour the formation of a donut like structure. However, the high substrate temperature leads them to diffuse and coalesce with each other leading to the formation of interconnected nanodonuts. These donuts will tend to merge to reduce their surface energy (larger island, lesser surface energy).

Nanomushroom Formation

Synthesis of novel nanostructures like nanomushroom and nanoflowers have been area of recent attention owing to their growth mechanism, although there is no conclusive report as such on the same. In our experiments, we achieved this growth at a very high temperature and flow rate. Although the substrate was coated with gold catalyst, the growth of octahedra along with with nanomushroom suggests inception of VS mechanism behind this growth. Fig. 11 below shows the growth of octahedra at different magnification. As it can be very clearly seen from the SEM micrograph at 5k, the growth of nanomushroom is uniform over the entire substrate and that there is on an average one visible octahedra per two nanomushrooms. The upper width of these nanomushrooms extends from 200-800 nm and these nanomushrooms are vertically standing. The edge of octahedra is ~200 nm long. At relatively high Argon flow rates, the process of precipitation and oxidation of indium, following its super saturation, may become faster than at low flow rate, leading to the formation of

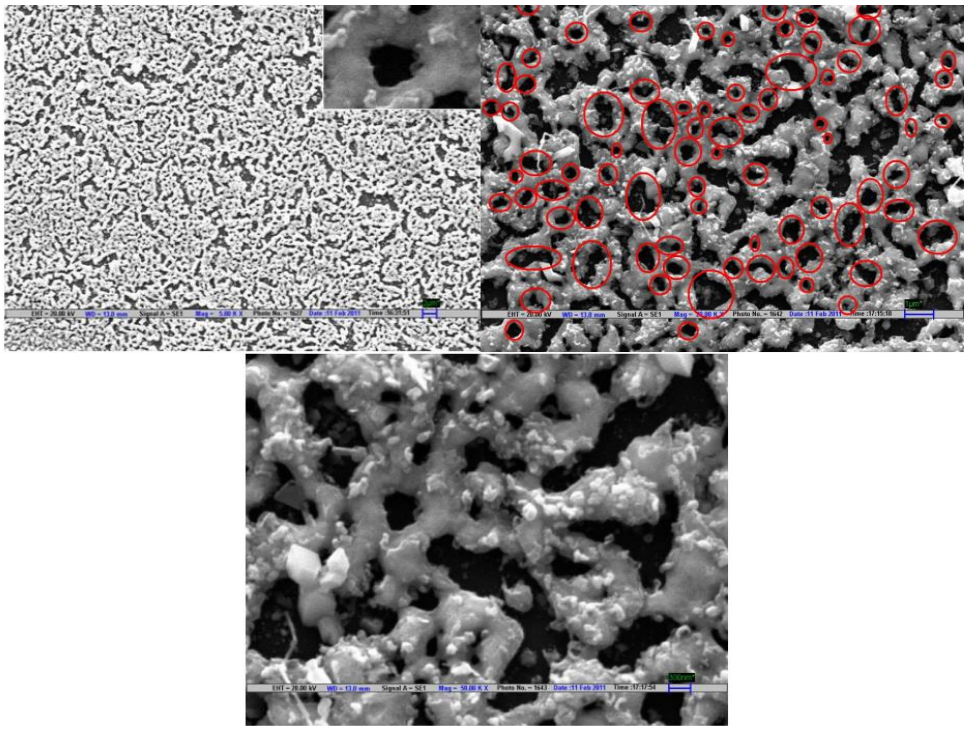

Fig. 10. SEM micrographs of Nanodonuts (a) 5k (Inset shows one single nanodonut unit) (b) 20k (c) 50k

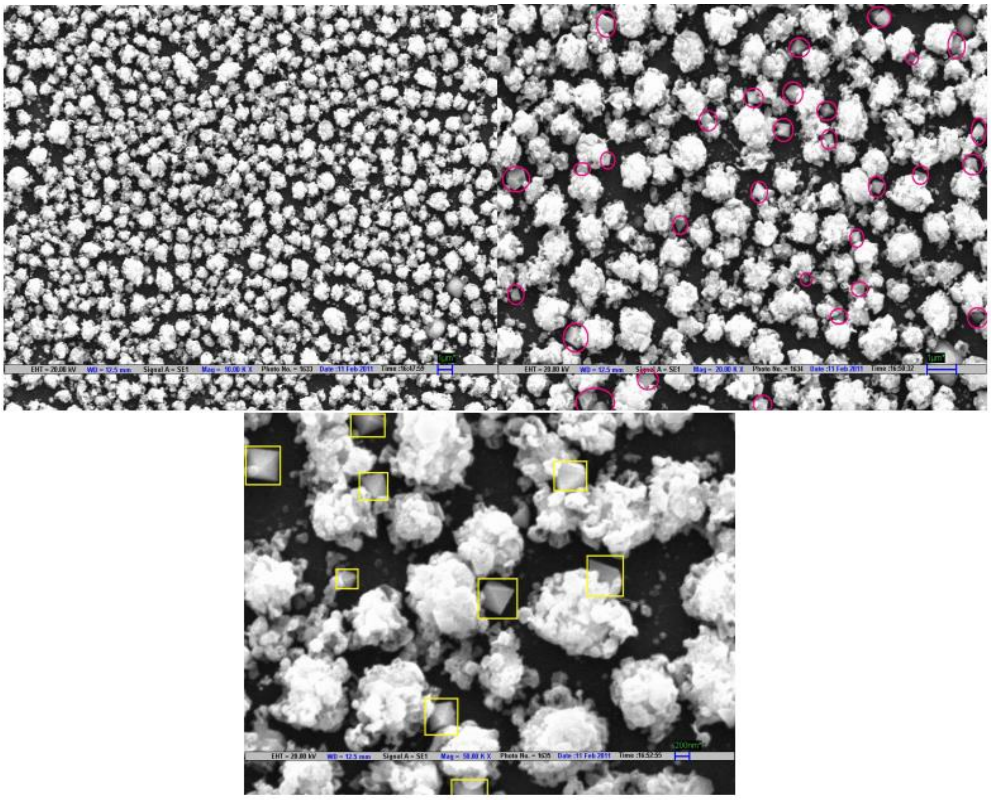

Fig. 11. SEM micrograph of the growth of nanomushrooms with octahedral (a) 5K (b) 20k (c) 50k; (the octahedral have been marked with pink and yellow respectively in (b) and (c))

Table 2. Nanostructure morphology and features obtained with hydrazine ambient under different experimental conditions in the CVD technique.

Source Temp. (^OC)	Argon flow-rate (*Sccm*)	Distance from boat (*in*)	Substrate Temp. (^OC)	Morphology	Features and average dimensions (Length, *L* and diameter, *D*)
900	50	0	885	Nanowires (NW) and Nanorods (NR)	NW: L< 7μm, D<35nm NR: L = 1.5±0.5μm, D~125nm
		1	855	Hexagonal faceted standing nanorods	L< 2μm, D<35nm
		2	805	Sparse growth	-
1000	50	0	960	High aspect ratio NW	L = 60±20μm, D = 50±10nm
		1	940	NRs and multipods	D = 50±5nm (each arm)
		2	880	Inter-penetrating NRs	-
1000	125	0	960	Multikinked NWs	-
		1	940	Kinked wire decorated nanowhiskers	-
		2	880	Agglomerates of kinked NWs	-
1000	200	0	960	NWs	L = 5±1μm, D = 60±20nm
		1	940	Short NRs	L = 2-4μm, D = 250±50nm
		2	880	Long NW-woven multipods	L = 5±1μm
1100	200	0	1050	Nanowhiskers	L = 2-4μm, D = 50-150nm
		1	1030	NWs	L = 1-4μm, D = 100-150nm
		2	960	Long Nanowires	10μm<L< 25μm
1200	200	0	1140	Interconnected Nanodonut web	D (Inner) = 100-400nm; Thickness = 100 nm
		1	1110	Nanomushrooms (NM) with octahedra	NM: Upper width = 200-800 nm; Octahedra : L~ 200 nm
		2	1060	Ultra long NWs	L< 50μm

irregular IO crystals around the In-rich Au–In alloys. It can be suggested that the growth in the beginning stages would have been a VS type followed by an uncontrolled growth due to the excess of incoming reactant species. However, the sequential steps behind the growth of nanomushroom structures and the actual growth mechanism needs to be explored further.

CONCLUSION

In summary, we have presented a facile and controllable method for the large-scale fabrication of a variety of IO nanostructures. This strategy of utilizing the presence of strongly reducing Hydrazine hydrate ambient in the CVD growth showed the different kinds of growth mechanisms in place. IO nanostructures were grown by systematically varying the carrier gas flow rate and the source temperature at three different downstream locations from the source. It was found out that both the carrier gas flow rate and substrate temperature have a significant effect on nanostrusture morphology. Furthermore, Flower like nanomushrooms and Nanodonut web of Indium Oxide were fabricated by intentionally altering the growth conditions to high temperature and carrier gas flow rate. Table 2 below summarizes the different growth morphologies obtained under different conditions in hydrazine ambient.

ACKNOWLEDGMENTS

We gratefully acknowledge Prof. B. R. Mehta and Dr. V N Singh from Department of Physics, IIT Delhi for their support throughout the project.

CONFLICT OF INTERESTS

The authors declare that there is no conflict of interests regarding the publication of this paper.

REFERENCES

1. Cheng G, Stern E, Guthrie S, Reed MA, Klie R, Hao Y, Meng G, Zhang L. Indium oxide nanostructures. Appl Phys A- Mater. 2006 Nov 1;85(3):233-40.
2. Cui Y, Wei Q, Park H, Lieber CM. Nanowire nanosensors for highly sensitive and selective detection of biological and chemical species. Science. 2001 Aug 17;293(5533):1289-92.
3. Kolmakov A, Moskovits M. Chemical sensing and catalysis by one-dimensional metal-oxide nanostructures. Annu. Rev. Mater. Res. 2004 Aug 4;34:151-80.
4. Huang XJ, Choi YK. Chemical sensors based on nanostructured materials. Sens. Actuators, B. 2007 Mar 26;122(2):659-71.
5. Hahn YB, Ahmad R, Tripathy N. Chemical and biological sensors based on metal oxide nanostructures. Chem. Commun. 2012;48(84):10369-85.
6. Gabriel J, Gruner G, Collins P, Swanson B, Wudl F, inventors; Nanomix, Inc., assignee. Electronic sensing of chemical and biological agents using functionalized nanostructures. US Pat. No. US 10/345,783. 2003 Jan 16.
7. Yamaura H, Jinkawa T, Tamaki J, Moriya K, Miura N, Yamazoe N. Indium oxide-based gas sensor for selective detection of CO. Sens. Actuators, B. 1996 Oct 1;36(1-3):325-32.
8. Du N, Zhang H, Chen BD, Ma XY, Liu ZH, Wu JB, Yang DR. Porous Indium Oxide Nanotubes: Layer-by-Layer Assembly on Carbon-Nanotube Templates and Application for Room-Temperature NH3 Gas Sensors. Adv. Mater. 2007 Jun 18;19(12):1641-5.
9. Zhang D, Liu Z, Li C, Tang T, Liu X, Han S, Lei B, Zhou C.

Detection of NO2 down to ppb levels using individual and multiple In_2O_3 nanowire devices. Nano Lett. 2004 Oct 13;4(10):1919-24.
10. Shukla S, Seal S, Ludwig L, Parish C. Nanocrystalline indium oxide-doped tin oxide thin film as low temperature hydrogen sensor. Sens. Actuators, B. 2004 Feb 1;97(2):256-65.
11. Zeng Z, Wang K, Zhang Z, Chen J, Zhou W. The detection of H_2S at room temperature by using individual indium oxide nanowire transistors. Nanotechnology. 2008 Dec 18;20(4):045503.
12. Kaur M, Jain N, Sharma K, Bhattacharya S, Roy M, Tyagi AK, Gupta SK, Yakhmi JV. Room-temperature H_2S gas sensing at ppb level by single crystal In_2O_3 whiskers. Sens. Actuators, B. 2008 Aug 12;133(2):456-61.
13. Kumar M, Mehta BR, Singh VN, Chatterjee R, Milikisiyants S, Lakshmi KV, Singh JP. The role of stoichiometry of indium and oxygen on gas sensing properties of indium oxide nanostructures. Appl. Phys Lett. 2010 Mar 22;96(12):123114.
14. Karn A, Kumar M, Singh VN, Mehta BR, Aravindan S, Singh JP. Growth of Indium Oxide and Zinc-Doped Indium Oxide Nanostructures. Chem. Vap. Dep. 2012 Sep 1;18(10-12):295-301.
15. Cho DH, Yang S, Park SH, Byun C, Yoon SM, Lee JI, Hwang CS, Chu HY, Cho KI. 21.2: Al and Sn-Doped Zinc Indium Oxide Thin Film Transistors for AMOLED Back-Plane. InSID Symposium Digest of Technical Papers 2009 Jun 1 (Vol. 40, No. 1, pp. 280-283). Blackwell Publishing Ltd.
16. Nguyen P, Ng HT, Yamada T, Smith MK, Li J, Han J, Meyyappan M. Direct integration of metal oxide nanowire in vertical field-effect transistor. Nano Lett. 2004 Apr 14;4(4):651-7.
17. Wang HW, Ting CF, Hung MK, Chiou CH, Liu YL, Liu Z, Ratinac KR, Ringer SP. Three-dimensional electrodes for dye-sensitized solar cells: synthesis of indium–tin-oxide nanowire arrays and ITO/TiO_2 core–shell nanowire arrays by electrophoretic deposition. Nanotechnology. 2009 Jan 12;20(5):055601.
18. Tsuruoka T, Liang CH, Terabe K, Hasegawa T. Optical waveguide properties of single indium oxide nanofibers. J. Opt. A: Pure Appl. Opt. 2008 Mar 27;10(5):055201.
19. Wu XC, Hong JM, Han ZJ, Tao YR. Fabrication and photoluminescence characteristics of single crystalline In_2O_3 nanowires. Chem. Phys. Lett. 2003 May 13;373(1):28-32.
20. Nguyen P, Ng HT, Yamada T, Smith MK, Li J, Han J, Meyyappan M. Direct integration of metal oxide nanowire in vertical field-effect transistor. Nano Lett. 2004 Apr 14;4(4):651-7.
21. Xu J, Wang X, Li C. Electrochemical-deposited In2O3 nanocrystals for H_2S detecting in air. Electrochem. Solid-State Lett. 2006 Jul 1;9(7):H53-6
22. Kim HW, Kim NH, Lee C. An MoCVD route to In_2O_3 one-dimensional materials with novel morphologies. Appl Phys A- Mater. 2005 Nov 28;81(6):1135-8.
23. Xu J, Wang X, Shen J. Hydrothermal synthesis of In2O3 for detecting H_2S in air. Sens. Actuators, B. 2006 Jun 26;115(2):642-6.
24. Kumar M, Singh VN, Mehta BR, Singh JP. Tunable synthesis of indium oxide octahedra, nanowires and tubular nanoarrow structures under oxidizing and reducing ambients. Nanotechnology. 2009 May 19;20(23):235608.
25. Zhong M, Zheng M, Ma L, Li Y. Self-assembly of versatile tubular-like In_2O_3 nanostructures. Nanotechnology. 2007 Oct 12;18(46):465605.